Target recognition by means of spaceborne C-band SAR data

Daniele Perissin, Claudio Prati

Dipartimento di Elettronica e Informazione
POLIMI - Politecnico di Milano
Milano, Italy
daniele.perissin@polimi.it

Abstract— **The relative low resolution (~25m x 5m on the ground) of spaceborne C-band SAR data as acquired e.g. by ESA sensors ERS and Envisat can be significantly increased (up to sub-meter precisions [1]) by processing coherently long series of images. Moreover, by analyzing the amplitude of the radar signal, the main radar characteristics of urban targets can be estimated and a system for automatic recognition of a set of scattering structures can be developed. In this work, we present the methodology and the results obtained on the test-sites of Milan and Shanghai by combining data acquired from ascending and descending passes and from parallel satellite tracks.**

I. Introduction

The present work moves its first steps from the Permanent Scatterers (PS) technique [2], a method developed in the last decade for detecting terrain deformations with millimeter accuracy from long series of SAR data. Such accuracy is achieved in correspondence of privileged targets, the so-called Permanent Scatterers. Even if the PS technique is now an operational tool used in both scientific and commercial projects, the physical nature of the targets is still subject of investigation [3], [4]. The knowledge of the scattering mechanism and a precise geo-location of the measurement points is a key step for a correct interpretation of displacement data obtained by PS interferometry and it can be extremely valuable to design effective monitoring programs in urban environment. For instance, the interferometric phase of a dihedral formed by the ground and a building wall can vary significantly in case of ground subsidence, but it does not change if only the building is affected by vertical motion [5]. Moreover, the classification of reflecting structures behaving as PS allows an a priori identification of the PS's looking at the structural details of buildings. Finally, if we know the PS physical nature, we can foresee their electromagnetic behavior under different acquisition geometries, frequencies and polarizations, and we can develop effective strategies for the integration of SAR data gathered by different sensors [6] (e.g. ERS, Envisat, Radarsat 1 and 2, TerraSAR-X, PALSAR, COSMO Sky-Med, etc.).

II. Target positioning

The processing chain that we developed for recovering information on the physical nature of urban targets consists of three main steps. The first one deals with the estimate of the precise 3D position of the target, the second one is the extraction of a set of features from the radar data that allow the characterization of the scattering structure. Finally, a system for the automatic recognition of the target typology can be developed.

The target precise 3D position can be extracted from SAR data (ground resolution about 25m x 5m for ERS) by means of multi-temporal interferometric techniques. The interferometric phase in fact depends on view angle changes (normal baseline and Doppler centroid frequency) as well as on slight frequency shifts (as between ERS and Envisat sensors) [1]. By processing the phase of many images, the relative 3D location of PS can thus be estimated up to sub-meter precisions. As an example, Figure 1 shows the 3D coordinates of PS's detected on the S.Siro Soccer Stadium in Milan from three different orbits, 2 descending and 1 ascending.

The quality of the obtained result suggested the exploitation of the estimated position of the scatterers to produce urban elevation maps. In particular, by analyzing the distribution of the height of the detected targets, it can be observed that most scattering structures lie on the ground. This fact can be fruitfully exploited to estimate the urban DTM. By selecting the PS's on the ground, and by applying a spatial kriging, the height of the terrain is resampled on a regular grid and the noise is filtered out. Figure 2 shows the DTM of Milan in a color scale range of about 6m around the low-pass topography of the city (a slight slope from North to South). The blue depressions in the image correspond to the water courses. The red area in the middle of the image identifies the historic center.

By means of the estimated DTM, the scatterer height is then referred to the ground level, obtaining very precise measurements (with respect to the system resolution) of the buildings elevation. Thus, considering that the image swath on the ground is 100km, a first raw tomography of a wide urban area can be produced at a very low cost. Moreover, the height with respect to the ground is a first information of the target physical nature.
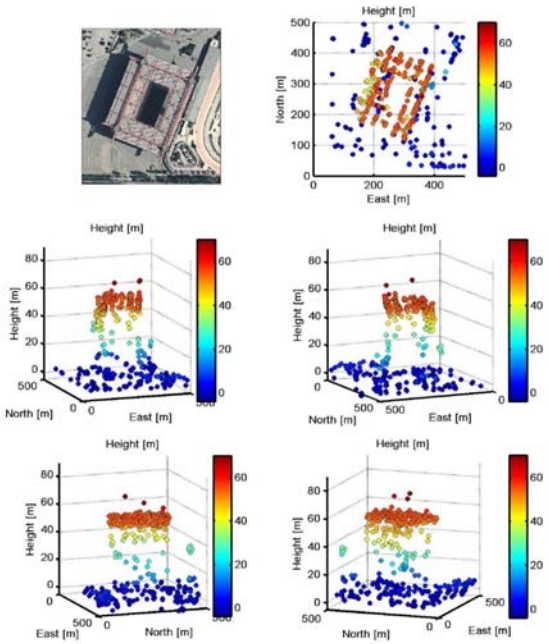
Figure 1. Aerial photo, planimetric coordinates and 3D views of PS's detected on the S.Siro Stadium in Milan from 2 descending tracks and an ascending one

Finally, the DTM obtained with the described technique has been compared with the ones produced using spot heights derived from photogrammetric analysis (courtesy of Milan Municipality) and using SRTM data. The spot heights are about 250.000 in the area of interest and the precison of the single measure is 30cm. Figure 3 reports the comparison between the PS and spot heights DTM's. The two height models have been resampled on the same grid and the difference between them is shown in the image on the left. The histogram of the difference values is reported on the right. The standard deviation between the two measures is less than 1m.
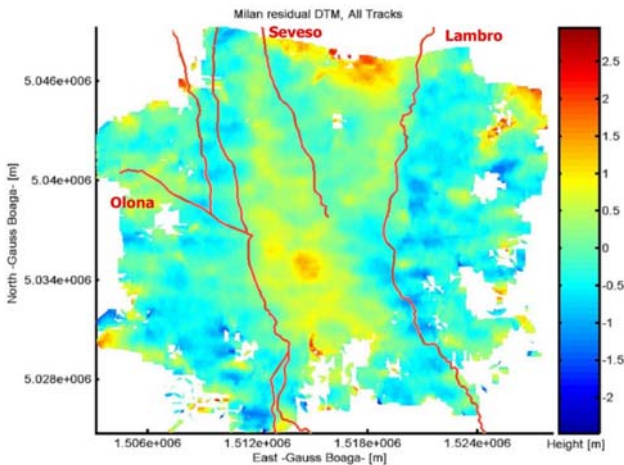

Figure 2. Milan DTM obtained from the height of PS's detected in three orbits (2 descending and 1 ascending) with the georeferenced watercourses of the city.

Figure 4 shows in analogous way the comparison between PS and SRTM data. As well known, SRTM height models are freely available and they have a spatial resolution of 90m (30m in the United States only). From Figure 4, the standard deviation of SRTM data with respect to the PS DTM is slightly less than 10m. Both the histogram and the height difference in planimetric coordinates show a positive bias in correspondence of the city center, where the buildings are higher and denser.

III. TARGET FEATURE EXTRACTION

The second step of our algorithm is the extraction of a set of features from the radar data that allow the characterization of the scattering structure of the target at hand. To this aim we analyze two main radar characteristics of the targets: scattering pattern and polarimetric behavior [3].

The target scattering pattern is analyzed by looking at the amplitude of the radar signal. The first information that can be extracted from the received amplitude is the Radar Cross Section (RCS). Then, many other useful hints can be derived by analyzing the variation of the RCS as a function of the acquisition parameters. Among them we take into account the geometry (normal baseline and Doppler centroid, DC), time and temperature. Variations of the RCS as a function of the acquisition geometry are related to the geometrical characteristics of the scatterer (extension and orientation in range and azimuth directions). The time domain has to be taken into account in order to identify possible temporary PS [8].
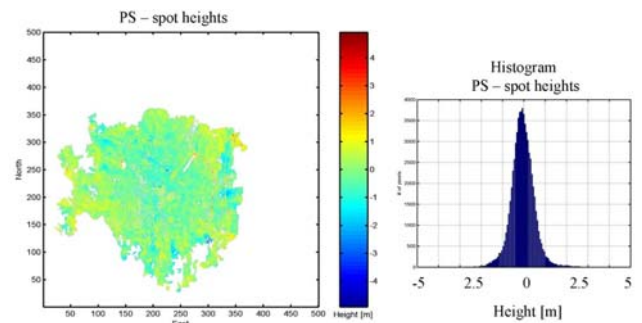

Figure 3. Comparison between DTM obtained from PS and photogrammetric spot heights data. Left: difference in planimetric coordinates. Right: histogram of the difference values.
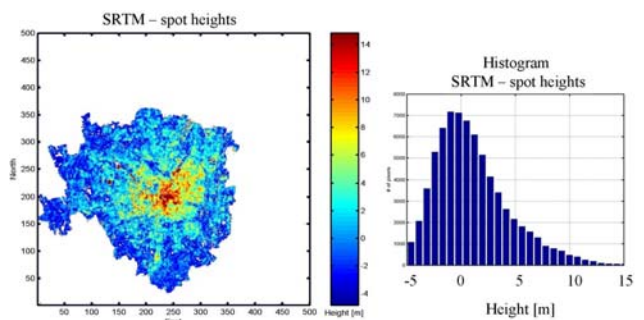

Figure 4. Comparison between DTM obtained from PS and SRTM data. Right: difference in planimetric coordinates. Left: histogram of the difference values.
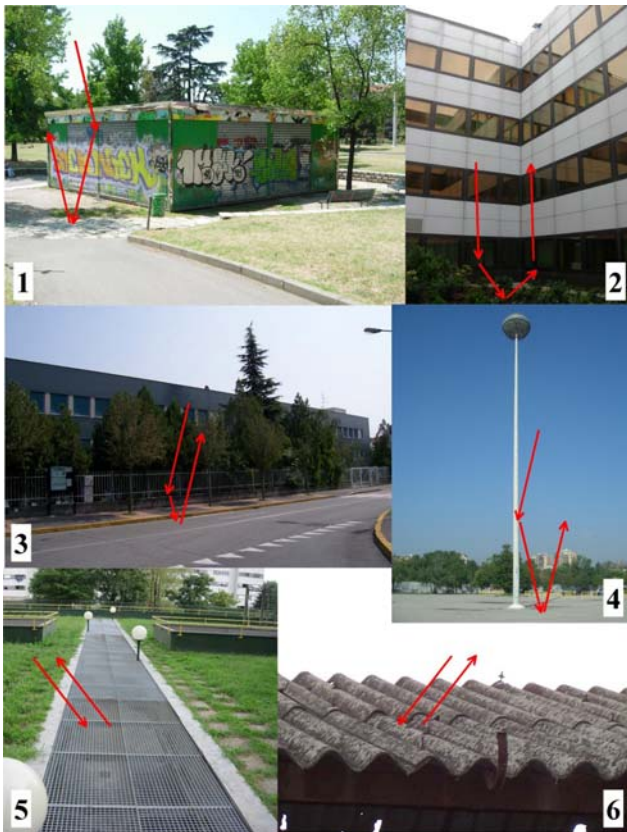
Figure 5. SAR target typologies in urban sites: 1) simple dihedral, 2) trihedral, 3) fence acting as resonating dihedral, 4) pole, 5) resonating metal grating, 6) backscattering roof

Finally, temperature-dependent RCS variations are used for detecting metal resonating structures (Bragg scattering) as gratings or fences. Such targets do not need to be physically oriented toward the sensor in order to be seen by the radar: the periodicity of their structure causes a resonance along the line of sight of the sensor. The distance between the periodic elements (in the order of magnitude of the wave length) is the key feature of the resonance and it causes RCS fluctuations as a consequence of thermal dilation.

The polarimetric behavior of the target is an other source of information on its physical nature. Rather than exploiting complex models, we analyzed it simply by means of an Envisat Alternating Polarization (AP) acquisition. In AP mode Envisat takes simultaneously 2 images with 2 different polarizations of the same area. Creating an interferogram between the two images (auto-interferogram), the interferometric phase depends only on the polarimetric response of the scatterers [7]. Thus the polarimetric auto-interferogram of a VV-HH acquisition can be exploited for discerning between odd and even bounces. A specular reflector (a mirror) behaves in the same way if illuminated with horizontal or vertical polarised signals, whereas a dihedral rotates the phase by π radians.

IV. TARGET CHARACTERIZATION AND RECOGNITION

Based on the previously described set of target characteristics (height with respect to the ground, geometrical dimensions, resonance attitude, bounces parity-disparity), urban SAR PS's have been classified in 6 main typologies: ground level resonating scatterers as floor metal gratings, elevated (roof-level) scatterers as tiled or corrugated roofs, dihedrals, resonating dihedrals as metal fences, poles and trihedrals.

Table I reports the characteristics of each target typology (L_{rg} range width, L_{az} azimuth width, φ_{AP} AP phase, RCS, k_T amplitude-temperature dependency, h height with respect to the ground). The last column is the percentage of detected targets in the urban site of Milan. Figure 5 shows some examples of targets in Milan as recognized in the validation campaign.

TABLE I. TARGET TYPOLOGIES

Target typology	Target characteristics						
	L_{rg}	L_{az}	φ_{AP}	RCS	k_T	h	%
Roof	+	+	0	$\propto$ dim	+	+	50
Grating	+	+	0	$\propto$ dim	+	-	11
Dihedral	-	+	π	+	-	-	13
Pole	-	-	π	-	-	-	11
Fence	-	+	π	-	+	-	7
Trihedral	-	-	0	+	-	-	8

A very simple system for the automatic recognition of the target typology can then be developed exploiting the information reported in Table 1.

V. APPLICATIONS

The processing chain has been tested and validated in the urban site of Milan by exploiting high-resolution optical data and in-situ surveys. It is reasonable to state that about 30% of targets can be recognized belonging to one of the 6 proposed scattering typologies with a good reliability index. We are now interested in considering two main applications that become possible knowing the PS's physical nature.

In the previous sections we have briefly mentioned that by knowing the target typology it is possible to properly interpret the measured deformation of the PS and it is possible to combine PS's detected from ascending and descending orbits, thus increasing the number of height measurements to generate DTM's. Here we tackle the problem of combining data acquired from parallel tracks. We consider two different cases, described by two real situations, Milan and Shanghai. In the first one we carry out an advanced PS analysis over Milan, we recognize a set of dihedrals and we observe them from a single interferogram of a parallel track. In the second case, we have only 12 images of the first track over Shanghai and 14 of the parallel one and we combine them incoherently in a common PS analysis, thus increasing the number of data.

Milan experiment.

Figure 6 briefly sketches the Milan case, reporting a result that validate the fact that dihedrals can be observed from parallel tracks. We assume that the phase of each PS is the sum of 4 main terms: height-dependent term, displacement-dependent term, atmospheric phase delay and noise [2]. We estimate height and displacement of each PS from the data
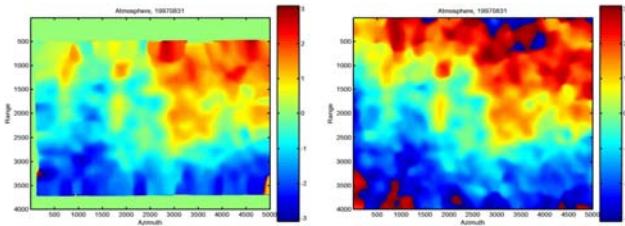
Figure 6. Atmospheric phase delay of the image 19970831 of Track 480 over Milan estimated: right) by means of a standard PS analysis over T480 data; left) by projecting the parameters of dihedrals estimated in the T208 PS analysis.

acquired in the 208 Track. Knowing which PS's are dihedrals, and knowing their geographical coordinates, we project them in an interferogram (19970831-Master in Figure 6) of the parallel Track (T480) and we subtract height and displacement estimated in the 208 Track. If our assumption is correct, residual phases depend only on atmospheric delay and noise. Thus, by spatial filtering the residuals we obtain the atmospheric artifacts, as shown in the left image of Figure 6. The image on the right in Figure 6 is the same atmospheric phase estimated from a standard PS analysis carried out on T480 data. The impressive agreement of the two images validates the assumption that dihedrals are coherently seen by parallel tracks.

Shanghai experiment.

Considering the ascending orbits of the ESA archived acquisitions over Shanghai, only 12 Envisat images of 268 Track and 14 Envisat images of 497 Track are available (as visible in Figure 7). Since at least 20 images are needed for carrying out a PS analysis, neither standard techniques nor the algorithm described in the previous case can be applied. But, assuming that dihedrals are visible from both parallel tracks, we can exploit them as a sub-set of super-PS and we can combine the data of the two tracks in a multi-track joint PS analysis. In order to implement the multi-track PS analysis the

images graph has to be modified from a single Master configuration (as e.g. in the ERS-Envisat coherent combination [9]) to a double Master one, as sketched in Figure 8. The results of the joint multi-track PS analysis are shown in Figures 9 and 10. Figure 9 in the upper part reports the reflectivity maps of the two parallel tracks with green circles in correspondence of the estimated multi-track dihedrals. Their multi-track coherence is shown in the lower part of the figure, together with an optical photo. Figure 10 groups the estimated height and average deformation trend of the detected dihedrals and an example of displacement time series (blue dots T268, red dots T497). As visible from Figure 10, besides the possibility of increasing the number of available acquisitions, a joint parallel track PS analysis allows to halve the revisiting time.

The obtained results suggested to apply for a patent on the use of dihedrals as a common PS network for SAR missions with different frequencies and incidence angles, that has been granted by the Italian patent office [10].

VI. CONCLUSIONS

In this work we have shown the possibility of super-resolving spaceborne C-band SAR data up to the development of a system for urban target automatic recognition. Six main urban target typologies have been characterized and a recognition process has been successfully implemented. Moreover, the identification of multi-track targets as dihedrals has been shown allowing the combination of parallel tracks, thus increasing the number of available images and reducing the revisiting time. Finally, the positioning capability of the described technique can be exploited to produce high accuracy urban DEM's, as validated by the comparison with photogrammetric data in Milan.
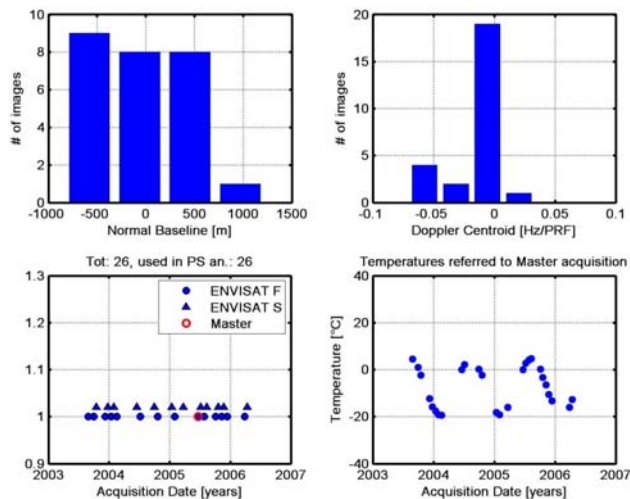
Figure 7. Multi-track (T268 and T497) dataset acquisition parameters. Above: left normal baseline, right DC frequency. Below: left temporal baseline, right synthetic temperature referred to the Master acquisition
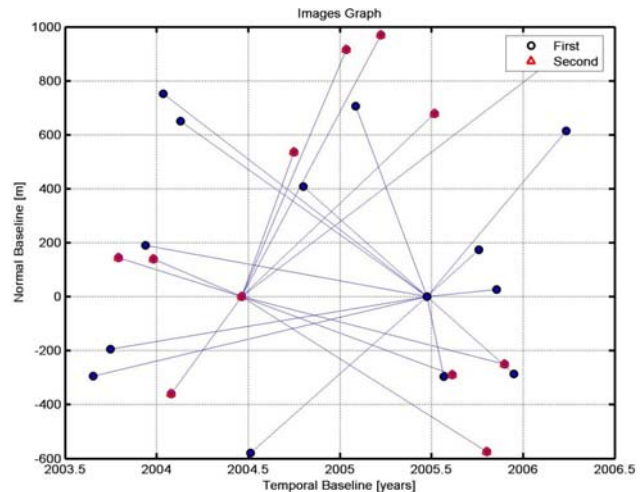

Figure 8. Multi-track (T268 and T497) dataset. Images graph (y-axis normal baseline, x-axis temporal baseline) with two different master images for the two different tracks.
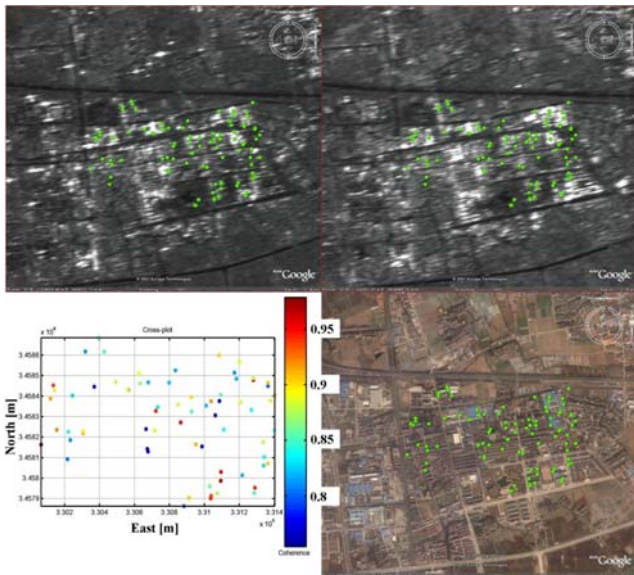
Figure 9. Above: reflectivity map of 2 different parallel tracks (T268 and T497) of a Shanghai urban area, with a green circle in correspondence of dihedrals commonly seen from the 2 geometries. Below: PS multi-temporal multi-track coherence of the detected dihedrals (left) and aerial photo with georeferenced PS positions.

and ERS data (provided under COPEESAT and Dragon projects), to the Milan municipality (divisione specialistica Sistemi Informativi Territoriali) for the spot heights data and to T.R.E. TeleRilevamento Europa for focusing and registering the SAR data.
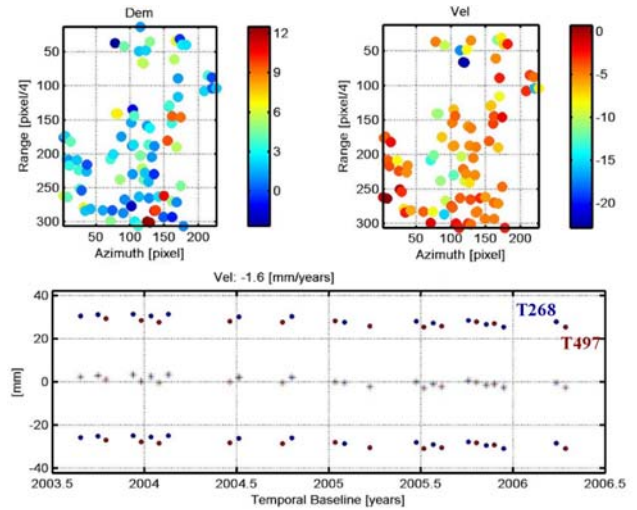

Figure 10. PS data of dihedrals detected in a Shanghai small area as observed from two different parallel tracks. Above: left) PS height; right) PS average deformation trend. Below: displacement time series for a dihedral as seen by the two tracks (blue: T268, red: T497).

REFERENCES

[1] Perissin D., Rocca F., "Urban DEM", Proceedings of FRINGE 2005, Frascati (Italy), 28 November - 2 December 2005

[2] Ferretti A., Prati C., Rocca F., "Permanent Scatterers in SAR Interferometry", IEEE TGARS, Vol. 39, no. 1, 2001.

[3] A. Ferretti, D. Perissin, C. Prati, "Spaceborne SAR anatomy of a city", Proceedings of FRINGE 2005, Frascati (Italy), 28 November - 2 December 2005.

[4] A. Ferretti, D. Perissin, C. Prati, F. Rocca, "On the physical nature of SAR Permanent Scatterers", Proceedings of URSI Commission Symposium - URSI 2005, Ispra (Italy), 20-21 April 2005

[5] Ketelaar V.B.H., Hanssen R.F., "Separation of different deformation regimes using PS-INSAR data", Proceedings of FRINGE 2003, Frascati (Italy), 1-5 December 2003

[6] A. Ferretti, D. Perissin, C. Prati, F. Rocca, "On the physical characterization of SAR Permanent Scatterers in urban areas", Proceedings of 6th European Conference on Synthetic Aperture Radar - EUSAR 2006, Dresden (Germany), 16-18 May 2006.

[7] Inglada J., Henry C., Souyris J-C., "Assessment of ASAR/IMS Multi-polarization Images Phase Difference in the Framework of Persistent Scatterers Interferometry", ENVISAT congress, Salzburg (Austria) 20-24 September 2004.

[8] Colesanti C., Ferretti A., Perissin D., Prati C., Rocca F., "Evaluating the effect of the observation time on the distribution of SAR Permanent Scatterers", Proceedings of FRINGE 2003, Frascati (Italy), 1-5 December 2003, ESA SP-550, January 2004.

[9] Perissin D., Prati C., Engdahl M., Desnos Y.-L., "Validating the SAR wave-number shift principle with ERS-Envisat PS coherent combination", IEEE Transactions on Geoscience and Remote Sensing, Volume 44, Issue 9, Sept. 2006 Pages: 2343 - 2351.

[10] Ferretti A., Perissin D., Prati C., Rocca F., "Metodo ed impianto di acquisizione di dati, uso di diedri per acquisizione di dati", italian patent N° MI2005A001912.